M Chernyshova et al.

Development of GEM detector for tokamak SXR tomography system: preliminary laboratory tests

Development of GEM detector for tokamak SXR tomography system: preliminary laboratory tests

Maryna Chernyshova[a], Tomasz Czarski[a], Karol Malinowski[a], Ewa Kowalska-Strzęciwilk[a], Jerzy Król[a], Krzysztof T. Pozniak[b], Grzegorz Kasprowicz[b], Wojciech Zabołotny[b], Andrzej Wojeński[b], Rafał Krawczyk[b], Piotr Kolasiński[b], Iraida N. Demchenko[c], Yevgen Melikhov[c]

[a]Institute of Plasma Physics and Laser Microfusion, 23 Hery, 01-497 Warsaw, Poland
[b]Warsaw University of Technology, Institute of Electronic Systems, 15/19 Nowowiejska, 00-665 Warsaw, Poland
[c]Institute of Physics, Polish Academy of Sciences, Al. Lotników 32/46, 02-668 Wasraw, Poland

The work presents the current status of design of the detecting system for poloidal tomography to be installed at WEST project tokamak for the first tests and verification of the detecting concept. The detecting system consists of two detectors which are expected to be installed in a poloidal section of the WEST project tokamak – one of planar and other of cylindrical geometry for the vertical and horizontal ports, respectively. In order to study the characteristics of the detectors and verify the proposed design first laboratory tests of the constructed detectors were performed. The results of the laboratory measurements of the prototype detectors with ^{55}Fe source and X-ray generator are shown. The detector amplification dependencies on high photon flux, start-up and applied high voltages are demonstrated. The cluster size of the generated anode charge and energy resolution are also provided. Two gas mixtures, Ar/CO_2 70/30 and $Ar/CO_2/CF_4$ were applied.

Keywords: Nuclear instruments and methods for hot plasma diagnostics; X-ray detectors; Electron multipliers (gas); Micropattern gaseous detectors.

1. Introduction

Necessity to develop new diagnostics for poloidal tomography focused on the metal impurities radiation monitoring, especially tungsten emission, has become recently inevitable. Tungsten is now being used for the plasma facing material on many machines, including on the WEST project, where an actively cooled tungsten divertor is being implemented [1]. This forced a creation of the ITER-oriented research programs aiming to effectively monitor the impurity level of tungsten in plasma. However, the situation is even more complicated as, due to interaction between particle transport and MHD activity, such impurities might accumulate which could lead to disruption, especially, in case of long pulse tokamaks. Therefore, an appropriate diagnostic tool has to be developed which will not just monitor the level of impurity but will also reconstruct its distribution. For this purpose, a Soft X-Ray (SXR) tomographic diagnostics with energy discrimination has been extensively considered for a while [2].

Detection system based on Gas Electron Multiplier (GEM) technology [3] has been recently proposed to be used as SXR tomographic system for ITER-oriented tokamaks and is under development by our group [4], [5], [6], [7], [8], [9]. The goal of our group is to design and construct such a new diagnostics for poloidal tomography focused on the metal impurities radiation monitoring, especially tungsten emission, in 2-15 keV energy region. A new GEM detectors based diagnostics was proposed to overcome an impact of the heavy modification of Tore Supra and installation of the vertical divertor and to improve the SXR system performance. This diagnostic system will combine spectral information on plasma radiation with good spatial resolution and should allow recovering fundamental information on plasma contamination and considering its effects on plasma scenarios.

The system is planned to be mounted to cover a poloidal section of the WEST tokamak with the vertically plasma observing detector to be situated inside a port with 83 tomographic lines, and the horizontally plasma observing detector to be located outside a port of 107 tomographic viewing lines. The main use of the SXR system measurements in the WEST physics Programme includes study of impurity content, in particular W, and study of MHD activity (modes and localization) where tomographic reconstructions are needed (2D phenomena). The targeted parameters of the developed GEM system are to fulfill the requirements of at least 1 kHz time resolution (the time scale of impurity transport) and 1 cm resolved detection of plasma volume at the equatorial plane for better tomography image. Comparing the previous Tore Supra SXR system [10] with the GEM based one under construction, it is envisaged that GEM detectors will provide more viewing lines, better spatial resolution, and mostly comparable time resolution and will bring also a new feature of spectral resolution.

The presented work is a part of development and research studies on design of the new diagnostics for poloidal tomography [5], [8], [11]. As a part of the tomography system, the GEM detector operation will take place in severe radiation surroundings. It is important, then, to verify their operation under targeted radiation

---

conditions. In this work initial laboratory results on the detector prototype performance are presented.

2. Experimental setup and methods

The presented in this work results were collected using constructed at IPPLM, Warsaw, triple GEM prototype detectors of 10x10 cm^2 detecting area. It consists of three GEM foils, which are both sides coppered thin insulator foils with small holes of double conical shape (50 μm of inner and 70 μm of outer diameter) densely packed with 140 μm pitch. The insulator's, polyimide foil, thickness is of 50 μm whereas Cu layers are of 5 μm thickness. The GEM foils were at a distance of 2 mm from each other. The conversion gap at the top of the first GEM foil was either 5 or 15 mm, and induction gap under the last GEM foil was set to 2mm. The entrance window on the top of the conversion gap was one-side aluminized Mylar foil of 12 μm thickness with about 0.2 μm conducting layer (cathode). The readout pixel structure (anode) was connected to ground via an analogue electronics (details are given below) for low photon rate, up to 0.01 kHz/mm^2, or to pico-ammeter (Keithley 6487) for the high photon rate tests (up to 2 MHz/mm^2). Applying a high voltage to the detector electrodes and GEM foils it is possible to multiply the primary charge, produced in a single event of photon absorption, whilst passing through the GEM foil and to transfer the electron part of it to the readout anode. Both 1D and 2D readout structures of the detector current signals were applied during the laboratory tests. The potentials to the GEM electrodes were provided either independently to each electrode or through a resistor divider chain. The detector was flushed with Ar/CO$_2$ 70/30 and Ar/CO$_2$/CF$_4$ 45/15/40 gas mixtures.

For the low photon rate measurements, all the data were collected using the serial data acquisition [12], [13] to obtain spatial and time characteristics for X-ray radiation. The assigned electronics aimed at collection the signal from a triple GEM detector, which has form of current in the range of hundreds of nanoamperes. To enable further processing, high gain transconductance amplifier was used. Unlike commonly used analog front end solutions, this stage simply converts current to voltage, without shaping. The data processing algorithms provides estimation of charges in numerical form from directly acquired samples, so shaping and integration is not needed. In order to meet Nyquist requirements and provide sufficient timing resolution without sacrificing of the signal shape, second-order low-pass filtering was applied in such way that attenuation of 50 dB is achieved at 35 MHz. ADC sampling rate is 77.7MHz at ENOB of 8 bits [14], [15]. Preservation of signal shape is essential for advanced deconvolution algorithms used at further stage.

All ADC samples exceeding the trigger level are acquired independently for each measurement channel. The acquired signal is analyzed within 40 samples. The first ten samples determine the offset level. The charge value is calculated as the sum of the next 20 signal samples. The criterion of regular signals is to fit in the time window. The last ten samples check overlapping signals. Distorted signals (overlapped or saturated) are marked by the special charge value and not taken for analysis.

Resulting serial data samples form a table of chronological triplets: [Q – charge value, P – channel number, T – triggered time]. Data packages are loaded sequentially to the DDR memory and finally are conveyed to the PC. Identification of a charge cluster (electron cloud projection on the readout anode) corresponding to a photon absorption is performed in two steps: 1) temporal selection of the simultaneous samples with zero or one sampling cycle difference; 2) spatial recognition of neighboring readout pixels within the set defined in the first step, and determination contributions of these particular charges in the total cluster charge for each readout pixel (e.g. 0.2, 0.5, 0.3). In this way a total cluster charge (as a sum of adjacent pixel charges exceeding the noise level) is defined, being a measure of the absorbed photon energy.

Only regular clusters without any defects (overlapped in time or space, saturated signals) are considered for histogramming. Regular clusters are counted in the four dimensional space determined by the planar cluster position, cluster charge value (energy) and time intervals. The pixel charge contributes to the total counts for a given pixel according to its charge weight within a total cluster charge. Final data processing concerns any 2D cross-section of cluster position (photon position), cluster charge (photon energy) and time interval. Consequently, radiation source characteristics are reflected in the cluster charge value and position distributions corresponding to the X-ray radiation energy and spatial image, respectively.

For the high rate measurements apparatus details and methodology were identical as described in [16].

3. Results of laboratory tests

First of all, start-up detector characteristics were checked after an initial applying HV to the all electrodes uncharged detector. The detector gain evolutions in time after switching on the HV are presented in Fig. 1 for two gas mixtures used. In case of ArCF$_4$CO$_2$ 45/15/40 the charging-up effect takes less time (approximately 1 hour) than for dual-component gas (about 5 hours). This is in accordance with the fact that adding CF$_4$ to the standard Ar/CO$_2$ gas mixture is known to substantially improve the time resolution of GEM detectors [17].
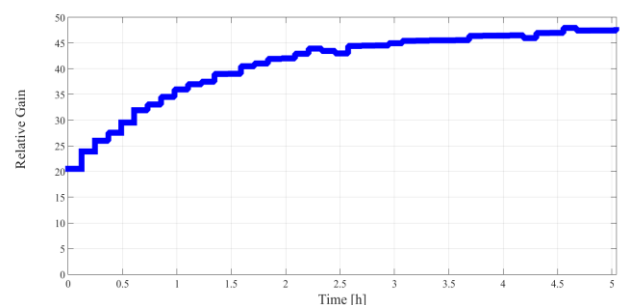

Fig. 1. Prototype detector gain evolution with time after switching on the HV.

After a stabilization of the detector stage basic characteristics as gain (effective amplification) and energy resolution were observed varying the HV applied to the GEM foils (Figs. 2, 3). The gain here is calculated as an ^{55}Fe source peak position on the electronics charge scale – effective detector gas amplification. Whilst energy resolution as a ratio of full width at half maximum to the iron peak position. As it is observed in Fig. 2, logarithmic gain dependence is fulfilled for almost all the HV region, excluding the highest values applied, where the detector operation steps over the proportional mode. Thus, reliable detector operation in the experiments is reachable within a certain range of HV, on condition that no pressure or temperature variations take the detector out of this region. Energy resolution dependence is different for the mixtures used (Fig. 3). Low content of Ar component provides to a worse resolution, similar to the lower gas flow rate.
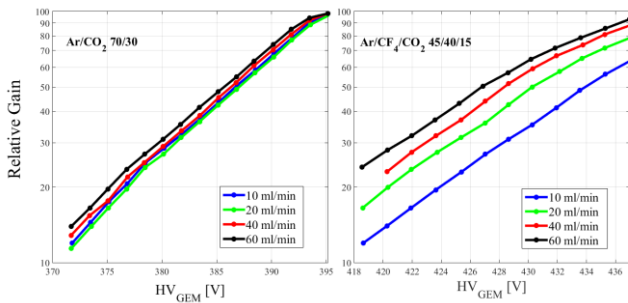

Fig. 2. Gain dependence on the applied HV to each GEM foil for different gas mixtures and flow rates.
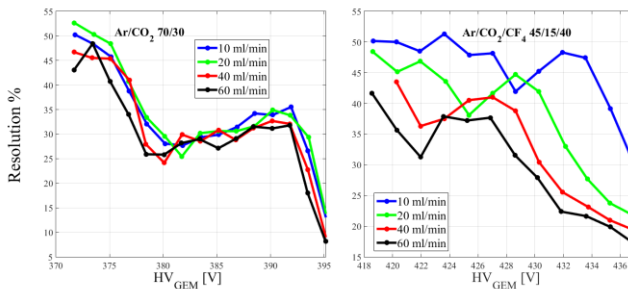

Fig. 3. Energy resolution dependence on the applied HV to each GEM foil for different gas mixtures and flow rates.

As a part of tomography system GEM detectors have to fulfill the tomography requirements. That is to provide a good spatial resolution of plasma image. This relates to a structure of the detector readout anode to be designed for such detector application. To fit a pixel size of the readout anode to a cluster size of the generated charge originating from a photon absorption, an experimental cluster size was estimated using the prototype triple GEM 1D strip detector with 0.8 mm strip pitch.

As a charge cluster of a given size may have different position relative to the strip geometry, it is assumed, therefore, that the distribution of the cluster center within one strip is uniform. The probability of arrangement to the segment is therefore proportional to its surface. For the strip width d and cluster of diameter $D < d$, one can specify a section of the strip, so that the cluster is completely contained inside this strip (single-strip

cluster). The probability of such an event is $P1 = (d - D)/d = 1 - D/d$. On the other hand, it is possible to experimentally obtain the probability $P1$ using histograms of the charges distribution for all clusters, H, and for single strip clusters, $H1$: the probability for every value of the cluster charge from the histogram can be represented as $P1 = H1/H$. By combining the experimental results and geometric analysis one can get the estimation of the average cluster size: $D = (1 - P1) d$, for each value of the cluster charge from the histogram.

The similar consideration can be performed for the general condition of $(n-1) d < D < n d$, where $n = 1, 2, 3, ...$ The probability of the cluster to spread out onto n successive strips is $Pn = (n d - D)/d = n - D/d$, consequently $D = (n - Pn) d$ is known if the experimental probability $Pn = Hn/H$ is measured, where Hn is the histogram for n-strips clusters.

The experimental histograms were obtained from the set of charge distributions covering the whole measuring range by adjusting the HV values on the GEM detector electrodes. The corresponding cluster size estimation for
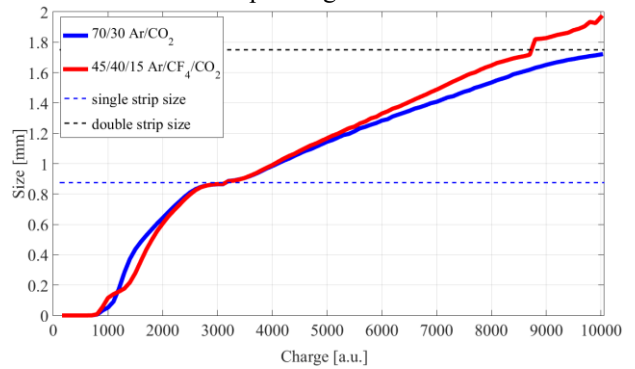

Fig. 4. Cluster size dependence on the generated charge for 0.8 mm strip pitch.

two gas mixtures is presented in Fig. 4. As can be seen with the lower fraction of the noble gas the cluster spot becomes smaller and does not exceed 2 mm for both mixtures. This result helped to define the strip size for the final detector optimizing the number of independent electronics channels and fulfilling at the same time the requirements for plasma spatial resolution.

GEM technology allows one to construct a gas detector of relatively high gain operating at radiation flux up to 10^5 mm^{2}s^{-1}. Due to the energy discrimination requirement, the detector should operate in the proportional mode with stable, relatively low, gas gain ($\sim 10^3$) with high dynamic range to prevent discharges and space-charge saturation. In order to fulfil these constraints, it is necessary to examine the GEM foil and select its relevant configuration. The detector rate capability for a standard double conical GEM hole was studied using a copper X-ray tube emitting 8 keV photons. The detector was irradiated with a collimated beam (1 mm in diameter) incident orthogonally to its window. The results of the irradiation are presented in Fig. 5 for two gas flow rates and the photon rate up to 2 MHz/mm^2. An average ionization energy for Ar gas is about 27 eV needed to produce one electron–ion pair. Thus, an initial primary charge generated by a photoelectron scattering in

the drift gap could be defined knowing the incident radiation energy and number of absorbed photons. The rate of the photon absorption, mostly happening in the conversion volume, was tuned by modifying the intensity of the X-ray generator. It was measured picking up the signals event by event from the bottom electrode of the last GEM [16]. Consequently, the effective electron
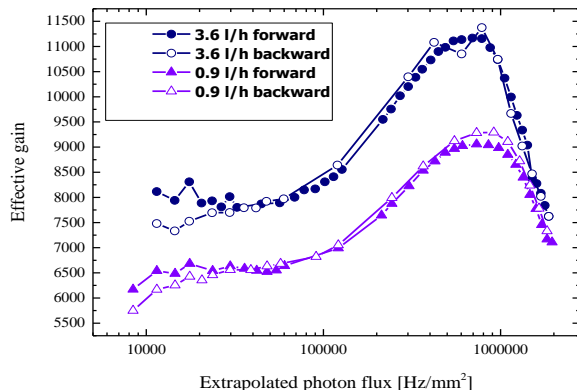

Fig. 5. Effective detector gain dependence on the photon flux.

gain was derived from the anode current normalized to the primary ionization charge and to the photon rate. It was measured after some time needed for the stabilization of charging up effect. About 290 primary electrons per event were generated. This electron gain is stable up to 100 kHz/mm^2 exhibiting further a remarkable rise. Considerable increase of the effective electron gain is observed starting from about 0.1 MHz photon intensity due to the significant space charge accumulation at the particular rate. It reaches a maximum at about 1 MHz/mm^2, after which it decreases. Different gas flows result in the higher gain for larger flows due to the gas purity impact on the creation of electron-ion pairs under irradiation. The obtained results are crucial for the development of the GEM based detector for the plasma radiation monitoring on account of its high emissivity. A similar experiment is planned to be performed for GEM foil with cylindrical holes in the nearest future. It is expected that for cylindrical GEM holes, the gain dependence on the photon flux will be much more stable. These data would finally allow defining the GEM hole type suitable for the plasma radiation monitoring diagnostics.

4. Summary

Spectrally-resolved SXR tomography is being developed and would be a very valuable tool for impurity transport monitoring and understanding, particularly W. GEM detectors are promising for this application and are resilient to neutron-induced damage. Preliminary laboratory tests of the prototype triple GEM detectors have been started recently. Different characteristics were collected during the tests. The gain and energy resolution dependencies on the varying GEM HV were shown. The cluster size was measured for two gas mixtures. The detector electron gain was measured for the photon fluxes up to 2 MHz/mm^2. Further tests are needed in order to

benchmark against another type of GEM foils. The obtained results will help in the final conclusion of the gas mixture choice and optimization of the detector operation.

References

[1] R. Hawryluk et al., Principal physics developments evaluated in the ITER design review, Nuclear Fusion 49 (2009) 065012 (15pp).

[2] D. Vezinet et al, Fast nickel and iron density estimation using soft X-ray measurements in Tore Supra: preliminary study, Fusion Science and Technology 63(1) (2013) 9-19.

[3] A. F. Buzulutskov, Radiation detectors based on gas electron multipliers, Instruments and Experimental Techniques 50(3) (2007) 287-310.

[4] J. Rzadkiewicz et al., Design of T-GEM detectors for X-ray diagnostics on JET, Nuclear Instruments and Methods A 720 (2013) 36-38.

[5] M. Chernyshova et al., Conceptual design and development of GEM based detecting system for tomographic tungsten focused transport monitoring, Journal of Instrumentation 10 (2015) P10022.

[6] D. Mazon et al., Design of soft-X-ray tomographic system in WEST using GEM detectors, Fusion Engineering and Design 96-97 (2015) 856-860.

[7] T. Nakano et al., Determination of tungsten and molybdenum concentrations from an X-ray range spectrum in JET with the ITER-like wall configuration, Journa of Physics B 48 (2015) 144023 (11pp).

[8] M. Chernyshova et al., GEM detector development for tokamak plasma radiation diagnostics: SXR poloidal tomography, Proceedings of SPIE 9662 (2015), 966231-35.

[9] S. Jednorog et al., Results of neutron irradiation of GEM detector for plasma radiation detection, Proceedings of SPIE 9662, Photonics Applications in Astronomy, Communications, Industry, and High-Energy Physics Experiments (2015) 96622Y.

[10] D. Mazon et al., Soft X-ray tomography for real-time applications: present status at Tore Supra and possible future developments, Review of Scientific Instruments 83 (2012) 063505-1-14.

[11] M. Chernyshova et al., Gaseous electron multiplier-based soft X-ray plasma diagnostics development: Preliminary tests at ASDEX Upgrade, Review of Scientific Instruments 87 (2016) 11E325-1-4.

[12] P. Kolasinski et al., Fast data transmission from serial data acquisition for the GEM detector system, Proceedings of SPIE 9662, Photonics Applications in Astronomy, Communications, Industry, and High-Energy Physics Experiments (2015) 96622J.

[13] P. Kolasinski et al., Serial data acquisition for GEM-2D detector, Proceedings of SPIE 9290, Photonics Applications in Astronomy, Communications, Industry, and High-Energy Physics Experiments (2014) 92902H.

[14] G. Kasprowicz et al., Fast modular data acquisition system for GEM-2D detector, Proceedings of SPIE 9290, Photonics Applications in Astronomy, Communications, Industry, and High-Energy Physics Experiments (2014) 92902F.

[15] A. Wojenski et al., Multichannel reconfigurable measurement system for hot plasma diagnostics based on GEM-2D detector, Nuclear Instruments and Methods B 364 (2015) 49–53.

[16] S. Franchino et al., Effects of high charge densities in multi-GEM detectors," arXiv:1512.04968v1 [physics.ins-det] (2015).

[17] M. Alfonsi et al., Operation of triple-gem detectors with fast gas mixtures, Proceedings of 8th International Conference on Advanced Technology and Particle Physics (ICATPP 2003): Astroparticle, Particle, Space Physics, Detectors and Medical Physics Applications (2003) 651-658.

[18] D. Vezinet et al., Principal physics developments evaluated in the ITER design review, Nuclear Fusion 49 (2009) 065012.

[19] M. Chernyshova et al., Development of GEM gas detectors for X-ray crystal, Journal of Instrumentation 9 (2014) C03003.